JOURNAL OF COMPUTATIONAL PHYSICS 12, 210–233 (1973)

An Integro-Differential Equation Technique for the Time-Domain Analysis of Thin-Wire Structures. II. Numerical Results*

A. J. POGGIO

Cornell Aeronautical Laboratory, Buffalo, New York 14221

E. K. MILLER

Lawrence Livermore Laboratory, University of California, Livermore, California 94550

AND

G. J. BURKE

M B Associates, San Ramon, California 94583

Received April 21, 1972

Presented here are the numerical results from a computer solution of the time-dependent thin-wire electric-field integral equation described in Part I of this paper. Both radiation and scattering problems are considered. The present results are validated by their Fourier transform to the frequency domain, where they are compared with independently computed data. A space–time sampling criterion is derived for predicting the highest frequency to which the time-domain calculations are accurate and found to be in accord with the numerical results. The time domain results are also shown to provide informative insights into the radiation characteristics of specific structures. Recommendations for further work are also presented.

INTRODUCTION

In Part I of this paper [1], we developed a time-dependent electric-field integral equation appropriate for structures composed of perfectly conducting thin wires. We introduced a numerical technique for solving these equations—concisely described as point-matching in space–time with second-order Lagrangian interpolation-basis functions and expanded on this in detail. We also discussed the advantages and disadvantages of time-domain analysis, provided computation time estimates for various operations, and derived ratios depicting the advantage of time domain over frequency domain analysis.

* Work performed under the auspices of the U.S. Atomic Energy Commission.

In this part we are presenting numerical results that typify time-domain scattering and antenna calculations and comparing these results with independently obtained data. The details of each calculation are given to help others who wish to compare results.

It is often said that the use of numerical techniques lessens the physical insight into a given problem. In an attempt to dispel this feeling we have, in specific instances in this paper, delved into the details of the computed temporal responses and have extracted certain features of the radiation phenomenon. In this manner, the analytical tool which has been developed is shown to also provide a meaningful exposition of the physics of the problem and, thus, lead to a deeper understanding of the mechanisms involved. The value of this type of information to physicists and engineers is inestimable.

In each of the cases to be considered, the wire structure is excited by an electromagnetic pulse. For scatterers, this pulse is in the form of an incident wave. For antennas, it is a time-dependent voltage across a finite source-region. The time-domain electric-field integral equation is then solved numerically to provide a time history of the induced current. From this, time-dependent radiated fields can be computed; or if there is an interest in frequency-domain information, the Fourier transform can be used to deduce the spectral characteristics of quantities such as input admittance. The capability to transform the time-domain data into the frequency domain also facilitates a verification of the computed results. Since experimental and independently computed time-domain results are relatively scarce, it is much more convenient to make the comparisons in the frequency domain, where there are ample experimental data and independently computed results.

This paper includes a study of the possible sources of error in this time-domain analysis technique. The requirements on space and time sampling densities are discussed and are shown to have a profound effect on the computed results, particularly with respect to the high frequency content of the waveforms. The highest frequency for which accurate results can be expected for a given structure is predicted using a space–time sampling criterion. The high frequency cut off in numerical accuracy as well as some lesser problems arising in the numerical evaluation are discussed, and it will become clear that each is surmountable at the expense of increased complication, computer time, or computer storage.

Excitation Function

Equation (8) of Part I strictly holds only for fields that are continuous and have a continuous derivative in space–time. For this reason we are somewhat restricted in our choice of excitation functions. However, this does not impose a severe

limitation, since most physically realizable sources have these characteristics of continuity; that is, we rarely find sources in nature that are truly discontinuous.

The excitation most commonly used in time-domain analyses via integral equations is the Gaussian pulse [2], which not only satisfies the continuity conditions but also reasonably approximates an impulse. The functional form for a Gaussian traveling wave is given by

$$G(z, t) = \exp\{-a^2[(z/c) - (t - t_{\max})]^2\}, \tag{24}$$

where z is the direction of propagation, c the propagation velocity, and a the spread parameter for a Gaussian waveform.

There might be an objection to using this time-dependent field as a source of excitation because its spectrum,

$$g(z, \omega) = (\pi^{1/2}/a) \exp(-\omega^2/4a^2) \exp\{-j\omega[(z/c) + t_{\max}]\}, \tag{25}$$

has a zero-frequency component. Although this is not a realistic description of a propagating wave generated by a realizable source (because the time integral of the radiated field of a finite source distribution which is zero for $t < 0$ and approaches zero for $t \to \infty$ must be zero), it does not violate any of the basic premises assumed in deriving Eq. (8). Furthermore, the $\omega = 0$ component of the excitation spectrum (the dc component) induces only a dc current component, which in turn does not contribute to the radiated field (as will be seen shortly). In fact, the use of a Gaussian pulse simplifies the calculations somewhat and allows us to estimate the impulse response in the sense of network theory, where the impulse response characterizes the network.

In some cases, we use another form of excitation: the time derivative of the Gaussian pulse. In the following examples, this form is applied only to a loop antenna where the loop's closed circuit characteristic can lead to a circulating current if the antenna is excited by a source voltage with a dc component. As will become obvious, the Gaussian pulse does not pose any special problems in calculating the far field, since the radiated field depends only on the time derivative of the antenna current at retarded times.

Determining the Radiated Field

In the forthcoming time-domain calculations, we compute the induced current according to Eq. (8) (Part I) but in a form suitable for numerical computation (such as Eq. [14], Part I). For antennas and scatterers alike, the magnitude of the incident or applied field $|\bar{E}^A(\bar{r}, t)|$ is specified in V/m, with the distinction that this field, in the antenna case, is generated by a finite voltage V_s applied over a finite

region Δ of the perfectly conducting structure, i.e., $| \bar{E}^A | = V_S/\Delta$. The radiation field due to the induced surface current density is then calculated from

$$\bar{E}_{\text{rad}}(\bar{r}, t_0) = \lim_{r\to\infty} r \left(\mu_0/4\pi r \int_s \{[(\partial/\partial\tau)\, \bar{J}(\bar{x}', \tau)] - [(\partial/\partial\tau)\, \bar{J}(\bar{x}', \tau) \cdot \hat{r}]\, \hat{r}\}\, da'\right), \quad (26)$$

where r is a distance from a suitably chosen origin, $\bar{x}'$ is a position vector in source coordinates, $\bar{J}(\bar{x}', t)$ is the induced current distribution on the surface of the conducting structures with elemental area da', and $(\partial/\partial\tau)\, \bar{J}(\bar{x}', \tau)$ represents the time derivative of the induced current at a given point on the antenna evaluated at the retarded time $\tau = t_0 + \hat{r} \cdot \bar{x}' \geqslant 0$.

For a wire structure, the current density $\bar{J}(\bar{x}', t)$ is replaced by $I(s', t)\hat{s}$, where $I(s', t)$ is the linear current in the axial direction, and da' is replaced by the incremental length ds'. Note that the time variable for the far field expression, denoted by t_0, is the real time t minus the propagation time from the origin to the far field point; i.e., $t_0 = t - (r/c)$.

Clearly this extraction of the propagation time from origin to field point can result in a radiated field at the far field point for $t_0 < 0$. For example, if there is a point on the structure which supports a current at $\tau = 0$ with $\bar{x}' \neq 0$, and if $\hat{r} \cdot \bar{x}' > 0$, then $t_0 < 0$.

On the other hand, the origin of the time coordinate for the radiated field could also be defined as the time a wave first reaches the observer. In this case, we define the observer time as $t_0 = t - t'$, with t' representing a propagation time as yet undetermined. Clearly if $t_0 = 0$ represents the starting point, then t' is defined by

$$t' = r/c + \min[\tau - (\hat{r} \cdot \bar{x}'/c)],$$

with the additional condition that $\bar{x}'$ and τ are such that $\bar{J}(\bar{x}', \tau) \neq 0$ for $t \geqslant 0$.

In this paper, we compute the radiated fields according to a time scale defined by $t_0 = t - (r/c)$. So that $t_0 = 0$ represents the initial time of observation in the far field, we introduce the additional shift, if required, when plotting the fields.

Spectral Characteristics

The system's response to a waveform of arbitrary shape can be determined from its response to a known waveform. For instance, let us assume that a response such as induced current or radiated field, denoted $0(t)$, has been computed for a known input waveform $G(t)$. For simplicity here, we consider only functions of a single variable t which are nonzero only for $t \geqslant 0$. For a linear system

$$0(t) = \int_0^t G(\tau)\, H(t - \tau)\, d\tau, \quad (27)$$

where $H(t)$ is the system response to a delta function (impulse response) but is thus far unknown. In the frequency domain, the transfer function—a unique description of a linear system—is given by

$$H(\omega) = [0(\omega)]/[G(\omega)], \tag{28}$$

with $0(\omega)$ and $G(\omega)$ the Fourier transforms of $0(t)$ and $G(t)$, respectively.

If the same system is excited by a waveform $I(t)$ the new response is written

$$F(t) = \int_0^t I(\tau)\, H(t - \tau)\, d\tau, \tag{29}$$

or equivalently as

$$F(\omega) = H(\omega)\, I(\omega). \tag{30}$$

Clearly, having once determined the transfer function $H(\omega)$ between two specific variables, we can calculate the response to any waveform by simple mathematical operations.

As an example, the knowledge of the current $I(s', t)$ induced on an antenna by a source $V_s(t)$ allows us to determine the structure's spectral characteristics. The input admittance of the antenna, which is defined by

$$Y(\omega) = I_s(\omega)/V_s(\omega), \tag{31}$$

where $I_s(\omega)$ and $V_s(\omega)$ are the source current and voltage spectra, respectively, is easily determined. From a single time-domain calculation, then, we have available the antenna input admittance over a range of frequencies. The accuracy of this computation, taking into account the discretized knowledge of $I(t)$ and the behavior of $V_s(\omega)$, will be considered in a later section.

The impulse response of a structure can thus be determined by computing the structure's response to a known (band-limited) waveform and determining the ratio of the spectra. The impulse response can also be estimated, for example, by using a sufficiently narrow Gaussian that approximates the delta function. Bear in mind, however, that this kind of approximation may not be generally acceptable when high accuracy results are required.

Sources of Error

The integral equation derived in Part I is solved by a point-matching technique in space–time and, as such, is subject to discretization errors. These errors arise because the equation is enforced at only a finite number of discrete points in space and time. The applied field, is, therefore, represented by a sequence of points: i.e.,

in a finite-dimension subspace of the infinite-dimension space in which the function is defined.

A fundamental requirement for accuracy of the solutions is that the sampled function truly represent the applied field in space and time. Furthermore, the sampling must be dense enough for the current variation in space–time to be accurately represented by the Lagrangian interpolation scheme of Part I. Well tested guidelines for sampling densities have not yet been established for space–time sampling, but we gain some insight into the requirements from guidelines set forth for time-harmonic methods [3, 4].

We now proceed to investigate how time and space sampling rates are interrelated and how they can affect accuracy for the high frequency components in a simple case.

The temporal sampling requirements can be determined by applying the Shannon–Kotelnikov theorem, which states that a band-limited function $s(t)$ is uniquely characterized by samples of $s(t)$ at intervals $(1/2f_c)$ apart if the sampling frequency f_c is equal to or greater than the highest positive frequency $f_{\max}$ in the $s(t)$ spectrum. Although many of the spectra of interest do not have a finite $f_{\max}$, we can, nonetheless, apply the sampling theorem with $f_{\max}$ denoting a point in the spectrum where its magnitude is much less than the maximum value. This then assures that the aliasing error due to frequencies above f_c is negligible.

From the temporal sampling theorem, we have

$$f_c = 1/(2\Delta t)$$

so that

$$f = c/\lambda \leqslant f_{\max} \leqslant f_c = 1/(2\Delta t) \tag{32a}$$

or

$$1/\lambda = 1/(2c\Delta t). \tag{32b}$$

This equation defines the relationship between the temporal step size and the frequencies or wavelengths that can be included accurately in a time-domain analysis and is established by considering the time-frequency relationship.

Equation (32b) is not the only criterion which must be established, since it does not consider the spatial sampling requirements. For the case where all segments Δz are of the same size,

$$\Delta z = L/N_s,$$

where N_s is the total number of spatial samples and L is the total wire length. If we introduce a notation from the frequency domain, where it is common to speak of samples per wavelength (N_λ'), we can write the number of spatial samples as $N_s = N_\lambda' L/\lambda$, so that

$$L/\lambda = (1/N_\lambda')(L/\Delta z). \tag{33}$$

Note that we have not as yet specified any relationship between N_λ' and the accuracy to be expected when solving an integral equation. However, we can state at this point, that from frequency-domain considerations, we choose an N_λ' for a class of structures which will provide a given degree of accuracy in the frequency-domain solution [3]. If we refer to this value of N_λ' as N_λ and observe that the solution will be accurate as well for L/λ less than the value calculated from Eq. (33), we define the sampling requirement dictated by spatial considerations as

$$L/\lambda \leqslant (1/N_\lambda)(L/\Delta z). \tag{34}$$

Clearly an accurate solution in the time domain requires that the length-to-wavelength ratios of all significant frequencies in the excitation function spectrum satisfy both Eqs. (32b) and (34). In compact notation, we then have

$$L/\lambda \leqslant \min[L(2c\Delta t)^{-1}, L(N_\lambda \Delta z)^{-1}], \tag{35}$$

where

$$\min(a, b) = a, \quad a < b$$
$$b, \quad a > b.$$

Let us now write Δt as an interval determined by the number of time steps (N_T) in a reference time span (T); that is, $c\Delta t = cT/N_T$. In particular, this cT can be chosen to be the length of the excitation pulse or, in case of a pulse of infinite extent, as the length between the two points containing the most significant part of the energy. Then Eq. (35) becomes

$$L/\lambda \leqslant (L/cT)\, N_T \min[\tfrac{1}{2}, (\alpha N_\lambda)^{-1}], \tag{36}$$

with $\alpha = \Delta z/(c\Delta t)$. The first part of the $\min(a, b)$ term refers to the temporal sampling requirement and the second part to the spatial sampling requirement. The maximum value of L/λ for which accurate results can be expected is then found from

$$(L/\lambda)_{\max} = (L/cT)\, N_T \min[\tfrac{1}{2}, (\alpha N_\lambda)^{-1}]. \tag{37}$$

The evaluation of Eq. (37), to establish the limiting value of L/λ for which the results will be accurate, requires a determination of the minimum of two quantities. In the interest of efficiency, it is best that both quantities be equal to the minimum, for then the number of samples in space and time are being minimized simultaneously to achieve the desired accuracy. Such a condition is specified by

$$\Delta z = 2c\Delta t/N_\lambda. \tag{38}$$

Since N_λ is generally greater than 2 (and for straight wires, circular rings, and other smoothly curved structures, $N_\lambda \sim 6$–10 for 10% accuracy), Eq. (38) shows that Δz is generally less than $c\Delta t$. This condition usually cannot be realized unless an interpolation scheme is used, since interactions between two spatial points within the same time step cannot be accurately modeled without time interpolation. The intent of the interpolation, of course, is to represent the dependent variable (the current) accurately over the entire space–time cone.

Besides the foregoing errors—which result from inaccuracies in the solution of the integral equation for the portions of the response pertaining to the high frequency part of the spectrum—there are others that emerge in the subsequent operations. These deserve some comment.

The high frequency components of the spectrum, as previously noted, are most subject to error in the time-domain calculations. Therefore, when computing a transfer function like $Y(\omega)$, one must be careful to observe all the high frequency limits because a $V_s(\omega)$ with rapid roll-off will heavily weight the high frequencies. Small inaccuracies, thereafter, could be greatly amplified, leading to inaccurate results.

Any discussion of errors from the Fourier transformation is beyond the scope of this paper. Moreover, these should not be of concern when the fast Fourier transform is used properly. Our procedure in this respect has been as follows:

The frequency-domain results are taken from time-domain data by Fourier transformation by use of the fast Fourier transform algorithm. The data records for that operation have involved 512 time steps, of which 240 have been taken from the calculated time history. The balance has come from extrapolation of the results. Since the time-domain data usually have indicated a late time ringing at a single frequency with exponential damping, the technique has been to use the late samples in the calculated records to determine γ and ω in $e^{-\gamma t} \sin \omega t$.

This automated procedure involves searching out successive maxima in the data record and then searching for intervening minima. If the absolute value of the minimum does not satisfy the $e^{-\gamma t}$ envelope (determined by fitting maxima), later portions of the data record are tested. If the test is satisfied, the value of W is computed. It should be noted that although the method readily discerns waveforms containing single frequency components of significantly different phasing (as in the early history in Fig. 4), it fails when the phase differences are small (as in the very late history in Fig. 4). Therefore, the values of γ and W as fit to the late history contain some errors although these must be small as evidenced by the data to be presented. In order to circumvent these problems, it would be preferable to fit a Fourier series (with exponential damping) to the data, but this is relegated to future work. In all cases presented in this paper γ has been large enough for the record to include sufficient samples for late times (essentially equal to zero) to minimize the aliasing problems in the Fourier transform.

Numerical Results

In this section, we shall consider the results of time-domain calculations. Our attention will be directed first to antenna structures and then to wire scatterers.

Antenna Structures

The first antenna to be discussed is the center-fed linear dipole. The length of this antenna (L) is 1 m, and its radius-to-length ratio is 0.00674 (i.e., $\Omega \equiv 2 \ln L/a = 150$). The temporal behavior of the source voltage impressed over a region $\Delta = L/11$ around the center of the antenna, in volts, is

$$V_s(t) = \exp[-a^2(t - t_{\max})^2], \tag{39}$$

with $a = 1.5 \times 10^9 \text{ sec}^{-1}$ and $t_{\max} = 1.43 \times 10^{-9}$ sec. The impressed electric field, in V/m, is then

$$|E^A(t)| = V_s(t)/\Delta = (11/L) \exp[-a^2(t - t_{\max})^2]. \tag{40}$$

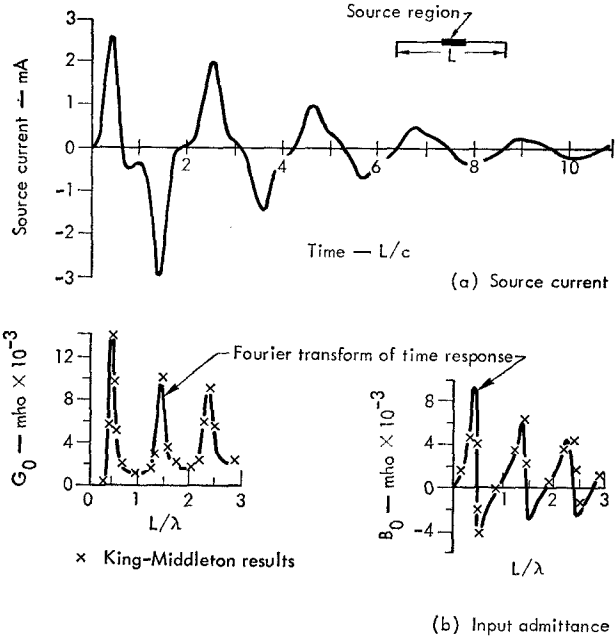

FIG. 1. Linear antenna with Gaussian source where the wire length is 0.5 m, the ratio of wire radius to length is 0.00674, the source width is $L/11$, and the number of spatial segments 22. $V_s = \exp[-a^2(t - t_{\max})^2]$ with $a = 1.5 \times 10^9$ and $t_{\max} = 1.43 \times 10^{-9}$ sec. King–Middleton results are plotted for comparison.

The antenna is subdivided into 22 spatial segments, the center two of which serve as the source region. The temporal step size (Δt) is set equal to $\Delta z/c = L/22c$, with Δz the spatial segment length. In this case, $\Delta t = 1.515 \times 10^{-10}$ sec. Because the Gaussian pulse has infinite support in the time domain, the starting point ($t = 0$) is defined, for practical reasons, at some reasonable level not equal to zero. Hence, $t = 0$ is generally chosen to correspond to the point on the leading edge of the Gaussian pulse which is 1 % of its maximum value.

Figure 1 typifies the results we obtain from the calculations which can be performed. In the upper part of the figure, the source current is plotted against normalized time; the horizontal axis is subdivided into length units normalized to the propagation velocity in free space. If we were to superimpose the input Gaussian pulse, the voltage and current would be seen to behave identically up to the first peak ($L/c = 0.5$); thereafter, the source current decays more rapidly than the input pulse. The explanation for this behavior in the region $0.5 \leqslant L/c \leqslant 1.0$ can only be electromagnetic coupling between the source region and other portions of the structure; it cannot be due to the reflected current pulse because the traversal time from source to end and return is approximately L/c sec.

The second major peak ($L/c \approx 1.5$) represents the arrival of the peak of the reflected current pulse at the source. Subsequent peaks occur at approximately odd integer multiples of $L/2c$. The slight discrepancies in current variation from these integer multiples can be attributed to the fact that the propagation velocity on the structure is somewhat less than that of free space.

The bottom part of Fig. 1 presents the input conductance and susceptance G_0 and B_0 versus the normalized length (L/λ), computed from the ratio of Fourier transforms of the source current and source voltage. For comparison, values from the King–Middleton theory [5] are included. From Eq. (37), with $cT = L$ and $N_T = 22$, the $(L/\lambda)_{\max}$ can be determined by using $N_\lambda = 6$ from Miller et al. [1]. For the structure under consideration, $(L/\lambda)_{\max} \approx 3.5$, as based on the smaller term in the $\min(a, b)$ term in Eq. (37). Since the space sampling term dictates $(L/\lambda)_{\max}$, we refer to this case as space-sample-limited. The discrepancy between the transformed and King–Middleton results for $L/\lambda > 3.5$ was evident and is not included in the figures.

Figure 2 is a computed time history of the antenna current over half the symmetrical, center-fed structure. It is not the current for the case shown in Fig. 1 but rather that for an identical dipole excited by a pulse with a spread half that for Fig. 1. This history is included for illustrative purposes. The dark horizontal lines represent the extent of the antenna, while the numbers identify the instant of time for which the current is plotted. Each integer refers to a multiple of $\Delta t = 0.152 \times 10^{-9}$ sec so that $L/c = 3.33 \times 10^{-9}$ sec $\approx 22\,\Delta t$. The pulse's progression along the structure is followed from the time of its first appearance at the source through its first reflection at the end and subsequent second appearance

at the source. It is from data like these, which are a direct result of the solution of the integral equation in space–time, that plots of the type shown in the upper half of Fig. 1 are derived.

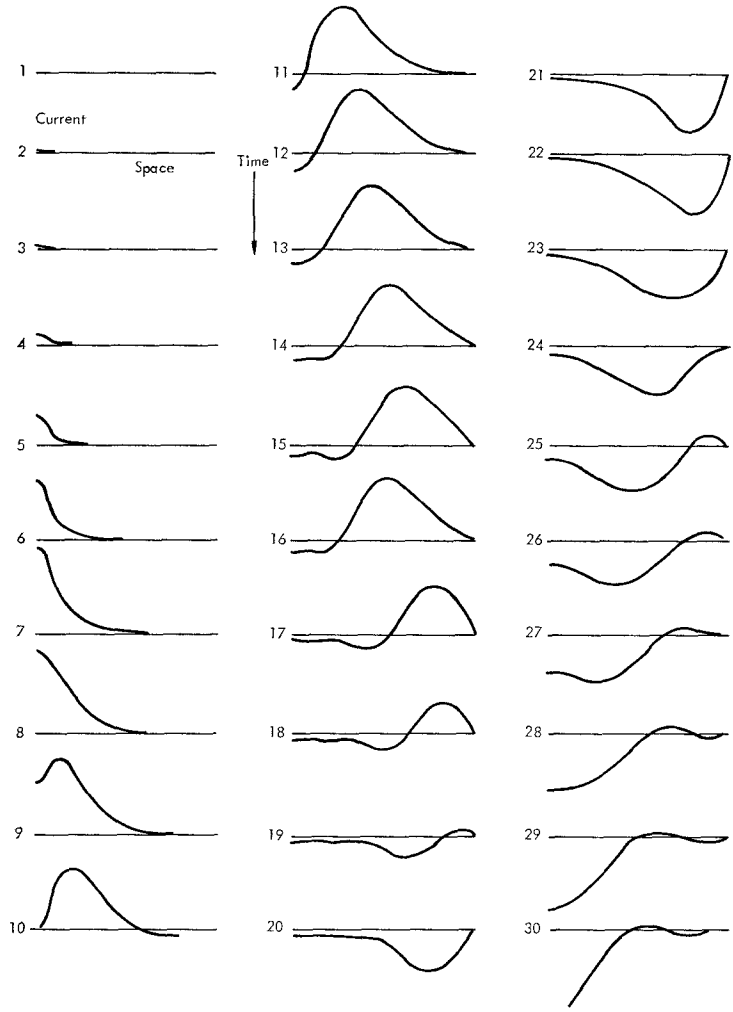

FIG. 2. Time history of dipole antenna current.

Figure 3 plots the broadside radiated field for the center-fed linear dipole. The temporal response, from the computed time history of the current and Eq. (26) specialized to wires, is shown in the upper half; the frequency-domain response

is shown in the lower half. The time scale in units of dipole length divided by the free-space velocity starts at $L/c = 0$, which is the instant the radiated field arrives at the observation point. The radiated field is driven by the temporal derivative

of the antenna current, as one would expect from inspection of Eq. (26). The predominant radiation comes from the source region (when the pulse first appears) and from the ensuing reflections which take place at the antenna ends.

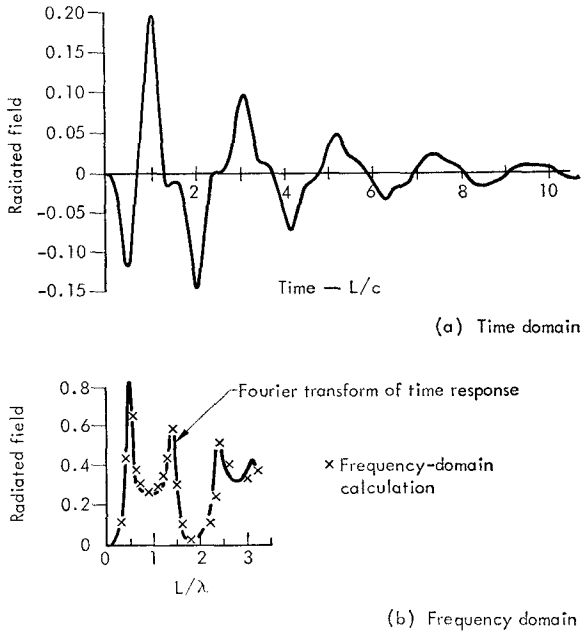

FIG. 3. Broadside radiated field of a linear antenna.

We will discuss this phenomenon in more detail when we consider off-broadside radiation. At this point, it is sufficient to point out that the field prior to arrival of the radiation due to end reflection is proportional to the negative of the source-region current.

In the bottom half of Fig. 3, the Fourier transform of the broadside radiated field is used for comparison with independently calculated results. The independent results in this particular case were obtained by a collocation solution of the thin-wire electric field integral equation [6] at the indicated frequencies. Again, discrepancies

the influence of this rather simple radiating system on the radiation of a Gaussian pulse.

As previously mentioned, the radiated field is a result of the temporal variation of the antenna current and is computed by a spatial integration over retarded values of the temporal derivative of current. If we envision the antenna current distribution to be a traveling wave with a Gaussian shape like that in Fig. 2, then the required time derivative is obtained from the Gaussian which, in the limit of narrow spread, becomes a doublet (the derivative of the Dirac delta function). Although for the case shown the Gaussian derivative is not very narrow relative to the antenna length, the use of the doublet representation points out the salient features of the phenomenon.

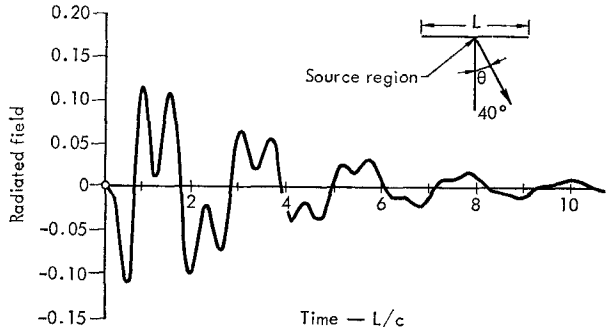

FIG. 4. Radiated field of a linear antenna with Gaussian source time dependence. The radiated field is at an angle 40° from broadside.

Figure 5 is included to illustrate further the effects seen in Fig. 4. As the wave first appears on the structure $t = 0+$, it causes the radiation seen at early times in Fig. 4. We refer to this first appearance of the wave at the observation point as the reference time, t_0. Once the peak of the Gaussian is passed, the derivative changes sign and serves to quench this source of radiation. We refer to the arrival of this peak as t_1.

To account for the next peak in the radiated field, at $t - t_1 \approx L/2c \sin \theta$ where $\sin \theta$ accounts for observing at an off-broadside position, let us first consider the boundary condition at the end of the antenna. Because the current is zero, the reflected wave must be of opposite polarity to the incident wave. As a result, the Gaussian suffers a continuous sign reversal at the end, as evidenced in Fig. 2. The time derivative of the current, which for the Gaussian traveling wave along the structure is similar to a doublet and, therefore, causes a negligible radiation field, reaches a point in time near the end of the antenna where its shape, instead of approximating a doublet, approximates the absolute value of the doublet

($t - t_1 \approx L/2c \sin\theta$). This causes significant radiation from the region near the antenna end and results in the second peak. The third peak is due to radiation from the other end of the antenna, while all subsequent peaks are due to reflections from alternating ends of the antenna as the wave travels back and forth.

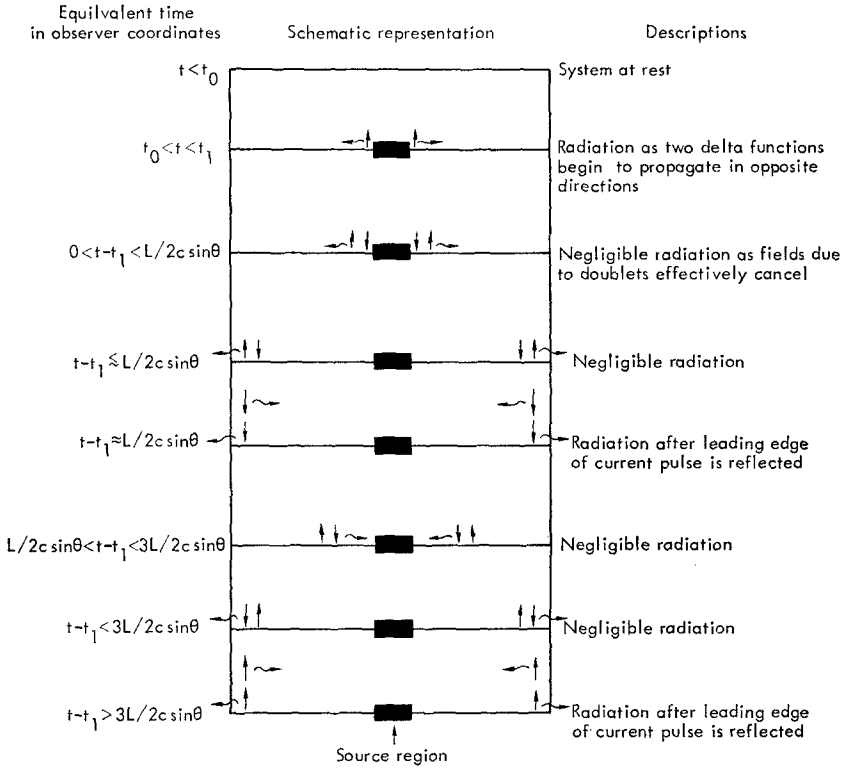

FIG. 5. Schematic representation of the radiation mechanism.

In general, the time of arrival of the peaks is given approximately by

$$t_n = t_1 + (L/2c)(n - 1 - \sin\theta) \qquad n, \text{ even},$$
$$t_n = t_1 + (L/2c)(n - 2 + \sin\theta) \qquad n > 1, \text{ odd}.$$

The time-dependent behavior of the loop antenna is considered in Fig. 6. For this particular case, the excitation voltage is assumed to have a temporal variation described by the time derivative of the Gaussian pulse. This particular excitation is chosen because it does not have a zero-frequency component and, therefore, does not excite the circulating current that would exist on the closed-circuit structure. The loop is modeled by 22 straight-line segments.

The upper part of Fig. 6 shows the source current as a function of time. The current shape here is very similar to that of the exciting voltage for $P/c < 0.5$; all perturbations to this close tracking are due to electromagnetic coupling effects and not to the arrival of the portions of the pulse which have circulated around the loop.

The input admittance of the loop antenna, plotted in the lower part of Fig. 6,

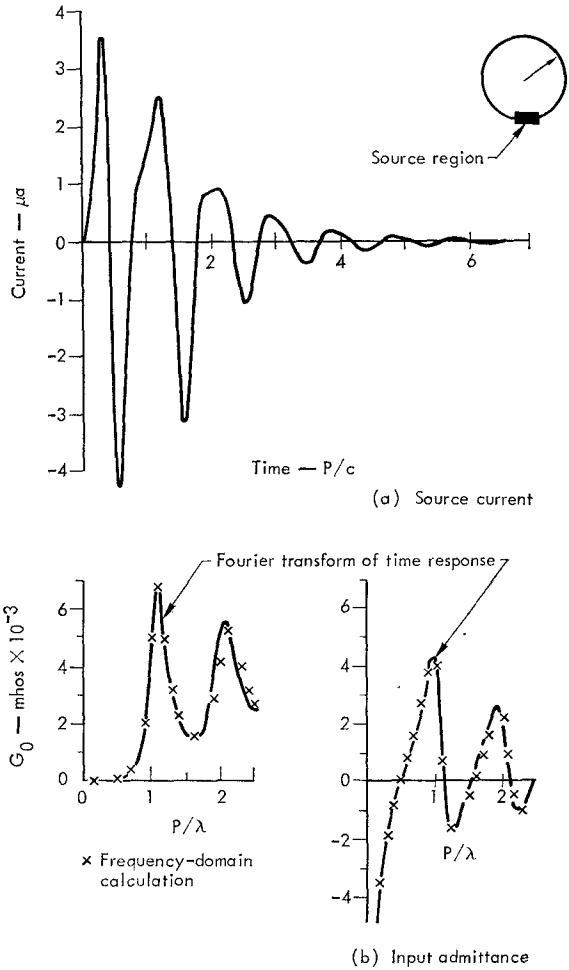

FIG. 6. Loop antenna with time derivative of Gaussian source where the circumference of the loop is 1 m, the source width is $P/11$, and the number of spatial segments 22. $V_s = 2a^2(t - t_{max}) \exp[-a^2(t - t_{max})^2]$ with $a = 1.5 \times 10^9$ and $t_{max} = 1.43 \times 10^{-9}$ sec. Frequency-domain calculations are plotted for comparison.

shows excellent agreement with the independently computed results for $P/\lambda \leqslant 2.5$, beyond which the time-domain derived values progressively depart from the correct results. For loop structures, modeling guidelines indicate that spatial samples in the frequency domain must be less than $\lambda/10$ in size ($N_\lambda = 10$), so the response of the highest frequency component of the incident pulse which can be accurately determined according to Eq. (37), with $cT \approx P$, is approximately $(P/\lambda)_{\max} \approx 2.2$. The $(P/\lambda)_{\max}$ values from theoretical considerations and our numerical results are, thus, in close agreement. Furthermore, since $L/zc\Delta t > L/N\Delta z$, we conclude that this case is also space-sample-limited.

The loop antenna calculation was repeated, using the Gaussian pulse of the previous computations. Although the temporal response of the source current was,

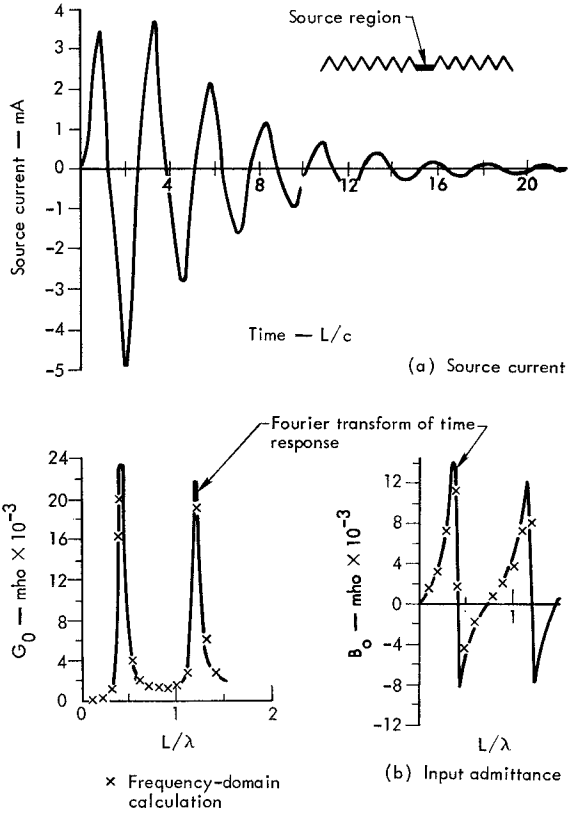

FIG. 7. Zig-zag antenna with Gaussian source time dependence; 22 spatial segments. The total wire length is 1 m and the dipole length 0.5 m. $V_s = \exp[-a^2(t - t_{\max})^2]$ with $a = 1.5 \times 10^9$ and $t_{\max} = 1.43 \times 10^{-9}$ sec. Frequency-domain calculations are plotted for comparison.

of course, quite different in this case and, in fact, reached a steady-state nonzero value for large time, all responses akin to spectral transfer functions (such as input admittance) agreed closely with the results obtained from the Gaussian derivative. This particular calculation can be viewed as a demanding test of the numerical procedure, and considering that the steady-state current became numerically stable in the fourth decimal place, the overall numerical accuracy of the approach is evidently quite good.

The final antenna to be treated here is the zig-zag dipole antenna excited with a Gaussian source. The computational results are shown in Fig. 7. By virtue of the cusps in the wire geometry, this antenna represents a particularly stringent test of the Lagrangian interpolation scheme described in Part I of this paper.

For such a structure, the effects of a current in a given segment during a given time step can be felt in adjacent spatial segments during the same time step using, as we have here, $c\Delta t = \Delta z$. Also, the high Q factor of this type of structure tests the ability of the computer program to predict not only late time behavior but also the highly peaked spectral transfer function (input admittance).

The source current behavior for this structure is plotted in the upper part of Fig. 7, while the input admittance is plotted in the lower part. The agreement is quite good for $L/\lambda < 1.3$, L being the total wire length. With modeling guidelines for zig-zag structures indicating that $N_\lambda = 20$ is required for relative errors less than 10%, we find from Eq. (37) that $(L/\lambda)_{\max} \leqslant 1.1$ is the approximate limit for accurate results in the frequency domain, again in reasonable agreement with the calculated data. As before, the results are space-sample-limited.

Wire Scatterers

The technique for determining the behavior of a given wire structure operated as a scatterer of an electromagnetic pulse in the form of a plane wave differs only slightly from that for determining its behavior when operated as an antenna. The difference lies only in the form of the applied field $\bar{E}^A$.

For an antenna, $\bar{E}^A$ is specified as due to a time-dependent voltage, that is, as a tangential electric field over a region at the surface of the wire. For scatterers, the applied field can illuminate the entire structure and is described as a Gaussian traveling wave, expressed in V/m, of the form

$$\bar{E}^A(z, t) = \hat{x} \exp\{-a^2[z/c - (t - t_{\max})]^2\}, \tag{41}$$

where the field x is polarized and the propagation direction is given by $\hat{z}$.

The radiated or scattered field is determined from using Eq. (26) and the computed time history of current. As described previously, an additional temporal transformation is introduced at the far-field point in order that the zero time point correspond to the instant a wave first reaches that observer.

The parameter of interest in the frequency domain is the radar cross section normalized to the square of the wavelength (normalized RCS), expressed in dB. It is also the most commonly available quantity for comparison of scattering results. The normalized RCS is defined by

$$\frac{\sigma}{\lambda^2} = \frac{\omega^2}{\pi c^2} \frac{| \bar{E}_{\text{rad}}(\omega) |^2}{| \bar{E}^A(\omega) |^2}, \tag{42}$$

with the dependence of σ/λ^2 on the incidence angle, observation angle, and polarization all suppressed. It is computed from the quotient of the spectra of the radiated field and the incident field. These in turn are determined by taking the Fourier transforms of the radiated field and the incident field.

Figure 8 shows the responses of a dipole operated as a scatterer for an incident electric field polarized along the wire axis, with the scattered field computed in the

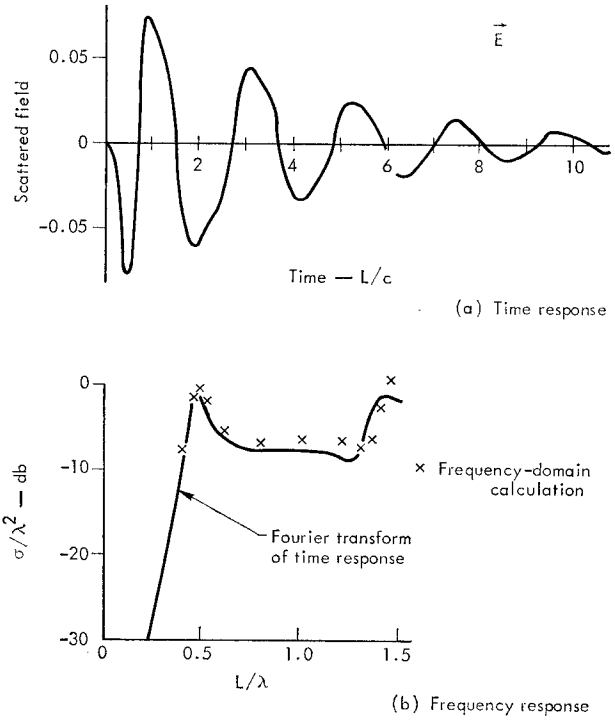

FIG. 8. Scattering of a Gaussian pulse by a dipole where the ratio of wire radius to length is 0.00667, the dipole length is 1 *m*, and the number of spatial segments 11. $\bar{E}^A = \exp\{-a^2[z/c - (t - t_{\max})]^2\}$ with $a = 1.5 \times 10^9$ and $t_{\max} = 1.43 \times 10^{-9}$ sec. Frequency-domain calculations are plotted for comparison.

backscatter direction for broadside incidence via Eq. (26). The constants associated with the Gaussian incident field are defined in the figure. From these constants, it is easily seen that the spatial extent of the applied pulse is approximately equal to the length of the scatterer. The normalized radar cross section is then computed from the Fourier transforms of the radiated and applied fields and Eq. (42).

A comparison with independent frequency-domain calculations is provided in the lower part of this figure. Note that the results begin to diverge for $L/\lambda \gtrsim 1.5$. This observation is consistent with the results already obtained for antennas, based on the space–time sampling density and the excitation pulse width in space relative to the structure's size.

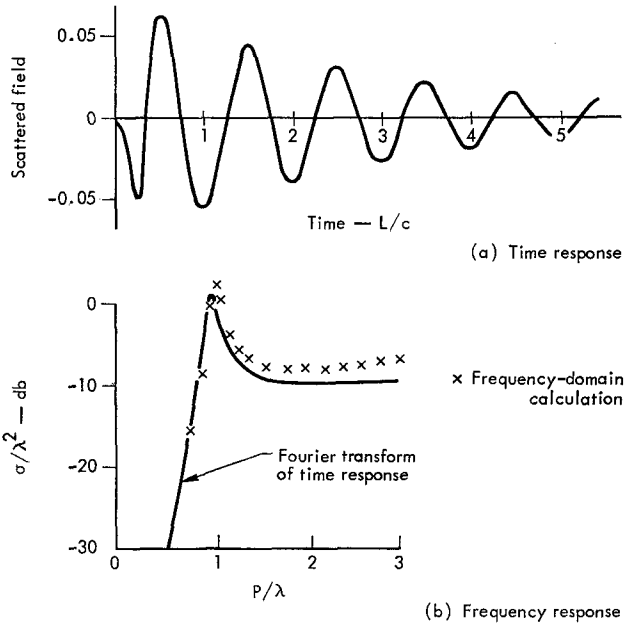

FIG. 9. Scattering of a Gaussian pulse axially incident on a ring whose circumference is 2 *m*. The ratio of wire radius to ring radius is 10^{-3} and the number of spatial segments 12. In this case, $\Delta t = 3.03 \times 10^{-10}$ sec $= \Delta P/c$, and $\bar{E}^A = \exp\{-a^2[z/c - (t - t_{max})]^2\}$ with $a = 1.5 \times 10^9$ and $t_{max} = 1.43 \times 10^{-9}$ sec. Frequency-domain calculations are plotted for comparison.

Figure 9 illustrates the response of a ring, modeled by a 12-sided polygon, to an axially incident Gaussian pulse. As evident from the time response (upper part of the figure), the far field of the loop settles into a ringing mode very rapidly and oscillates at the fundamental frequency (with exponential decay). This indicates a sharp peaking in the frequency response, and, indeed, this is observed in the

lower part of the figure, where the results are compared with independent data. A deterioration is again noted at the higher frequencies, brought on by the finite number of samples. Using Eq. (37) with $P/cT \approx 2$, $N_T = 12$, and $N_\lambda = 10$, we obtain $(P/\lambda)_{\max} \approx 2.4$, with spatial sampling the limiting factor.

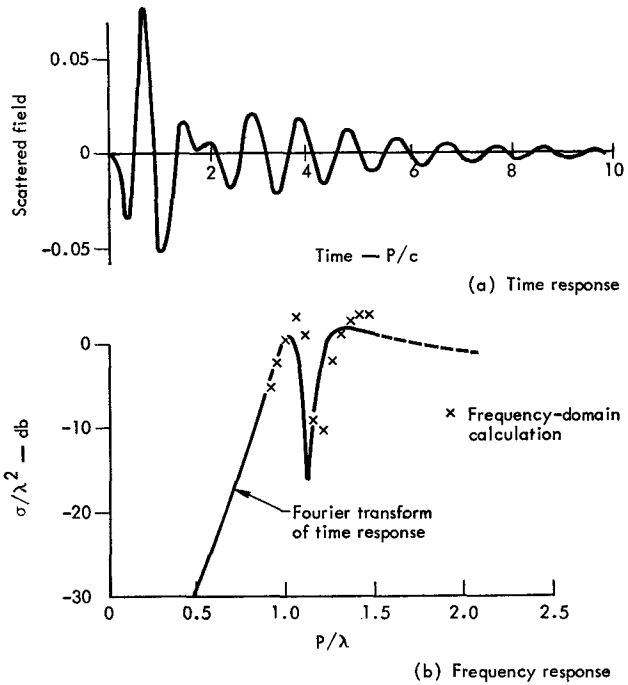

FIG. 10. Scattering of a Gaussian pulse by two concentric rings where the circumference of the large ring is 1 m, the ratio of ring radii is 1.25, the ratio of wire radius to ring radius is 0.03, and the number of spatial segments (each ring) is 12. In this case $\Delta t = 2.777 \times 10^{-10}$ sec, and $\bar{E}^A = \exp\{-a^2[z/c - (t - t_{\max})]^2\}$ with $a = 1.5 \times 10^9$ and $t_{\max} = 1.43 \times 10^{-9}$ sec. Frequency-domain calculations are plotted for comparison.

As an extension of the single-loop results, we show in Fig. 10 the responses of two coplanar, concentric rings to an axially incident Gaussian pulse. An amplitude-scaled version of the incident pulse is shown in the time response. The temporal behavior of the radiated field is somewhat more erratic than the single loop for early times ($t < 2.5\ P/c$) but settles down to a simple ringing mode for later times.

Another observed characteristic is the much lower field strength seen in the double-loop case for times greater than $1.5\ P/c$. The reason for this will become obvious when we look at the time-dependent currents on the rings. The normalized

radar cross-section curve exhibits reasonably good agreement with independent results for $P/\lambda < 1.0$, deterioration occurring above that point. A frequency shift seems to have taken place, but aside from this it is encouraging to note that the null in the response is well predicted. The maximum P/λ for accurate results is computed according to $P/cT \approx 1$ and $N_\lambda \approx 10$ so that $(P/\lambda)_{\max} \approx 1.2$. Note that this falls near the deep null in the normalized RCS.

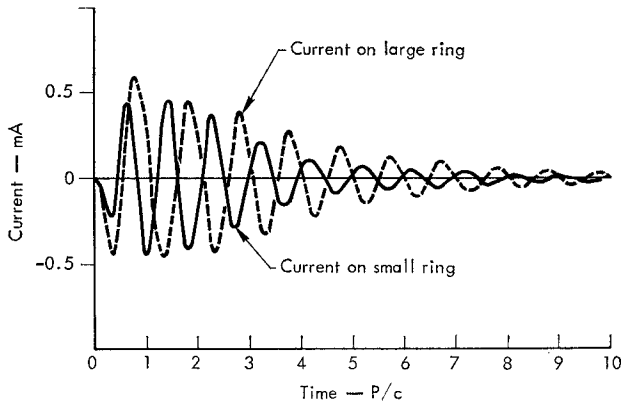

FIG. 11. Current on two concentric rings due to incident Gaussian pulse.

In Fig. 11 we see the current at the point on each ring where the incident magnetic field is orthogonal to the ring as a function of time. For very early times, the currents are independent; that is, there is no interaction between the rings. The currents, thus, start out in phase but lose their phase correlation as the combination of mutual electromagnetic coupling between the rings and their differing natural frequencies take effect. In fact, for times greater than $1.5\,P/c$, the currents are almost in phase opposition (though differing somewhat in amplitude and period), thus, giving rise to oscillations similar to a transmission line (push–pull) mode. The strong peak in the scattered fields at early times and its rapid decay to a lower oscillation level are thereby explained.

As a final example of time-domain calculations, we show in Fig. 12 the response of a circular crown band to an axially incident Gaussian pulse. The crown band is a zig-zag wire structure 85 in. in length, wrapped on the surface of a cylinder 25.13 in. in circumference. This example is particularly well suited to our discussions since it represents a stringent test of the ability of the interpolation scheme described in Part I to allow arbitrary space–time sampling. In fact, for this case one can easily see that $c\Delta t > \Delta R$; that is, the distance a wave propagates in one time step is greater than the distance between sample points. This in turn allows interactions between various segments within the same time step.

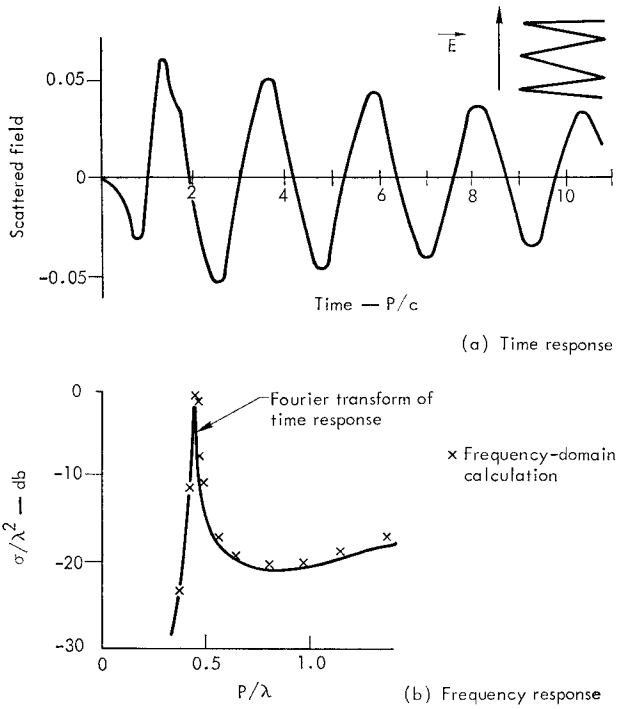

FIG. 12. Scattering of a Gaussian pulse by a six-point crown band 25.13 in. in circumference; 22 spatial segments. The total wire length is 84 in. and wire radius 0.0625 in. Segment length $\Delta z = c\Delta t$. $\bar{E}^A = \exp\{-a^2[z/c - (t - t_{max})]^2\}$ with $a = 2.0 \times 10^9$ and $t_{max} = 1.06 \times 10^{-9}$ sec. Frequency-domain calculations are plotted for comparison.

The crown band is also a fine example of a high Q scatterer with a highly peaked response curve in the frequency domain. The slow wave characteristic of the zig-zag structure is exhibited by the ringing period of the radiated field, which in turn is reflected by the resonance in the normalized radar cross section. Agreement with independently computed results is quite good for $P/\lambda < 1.8$, again in correspondence with the limit imposed by Eq. (37) where $N_\lambda = 20$, $N_T = 11$, $L = 85$ in., $cT = P$, and $\alpha = 1$.

CONCLUSIONS

The numerical technique developed in Part I of this paper has been applied to several wire structures. The time-domain results, obtained by numerically solving an integral equation in space–time, have been compared with available

data in the frequency domain by Fourier transformation. The usefulness of the Lagrangian interpolation scheme, which permits the dependent variables to be determined accurately in the entire space–time cone and, therefore, allows the interactions between different spatial segments within the same time step to be accurately described, has been illustrated by treating structures with cusps where the distance between spatial segment centers could be less than $c\Delta t$. This flexibility allows for analysis of more complicated structures at the minor expense of requiring a sparse matrix to be inverted at the initial stage of the computation.

A simple formula for determining the highest frequency for which the results are accurate has been derived. It can be widely used and has been shown to predict $(L/\lambda)_{\max}$ with reasonable accuracy. However, this formula has been validated only for cases where spatial-sample limiting was the dominant factor.

The study presented here is one step towards the time-domain analysis of general thin-wire structures. The areas for future work are many. First and foremost, accuracy-modeling guidelines of the type available in the frequency domain must be established for various classes of structures and different levels of interpolation. Also, techniques for handling multiple-wire junctions must be developed so that more complicated structures can be analyzed.

Since the characteristics of antennas can be greatly influenced by the presence of other obstacles (or the earth), we should also consider the general problem of time-domain analysis of antennas in the presence of a dissipative half-space. As a further extension, techniques such as Bennett's [7] for solid conducting bodies with straight wire appendages must be developed for analyzing solid conducting bodies with arbitrarily shaped wire appendages. Finally, problems involving nonlinearly loaded antennas and scatterers deserve detailed consideration.

ACKNOWLEDGMENT

The results presented in this paper were obtained when all the authors were staff members at M B Associates, San Ramon, California.

REFERENCES

1. E. K. MILLER, A. J. POGGIO, AND G. J. BURKE, An integral equation technique for the time-domain analysis of thin-wire structures. I. The numerical method, *J. Computational Phys.*
2. C. L. BENNETT AND W. L. WEEKS, Transient scattering from conducting cylinders, *IEEE Trans. on Antennas and Propagation* **AP-18** (1970), 627.
3. E. K. MILLER, G. J. BURKE, AND E. S. SELDEN, Accuracy-modeling guidelines for integral equation evaluation of thin-wire scattering structures, *IEEE Trans. on Antennas and Propagation* **AP-19** (1971), 534.

4. A. R. NEUREUTHER, B. D. FULLER, G. D. HAKKE, G. HOHMANN, C. C. HUNG, H. A. KOLHOR, B. R. KENDALL, A. D. KREISS, J. P. SCHERER, A. P. SHOMO, AND T. C. TONG, "A Comparison of Numerical Methods for Thin Wire Antennas," URSI meeting, Boston, Massachusetts, Fall 1968.
5. R. W. P. KING, "The Theory of Linear Antennas," Harvard University Press, Cambridge, MA, 1956.
6. A. J. POGGIO AND E. K. MILLER, Integral equation solutions of three-dimensional scattering problems, Technical Rpt. TM-70/20 M B Associates, San Ramon, CA, *in* "Numerical Techniques for Electromagnetic Boundary Value Problems" (R. Mittra, Ed.), Pergamon Press, New York, 1972.
7. C. L. BENNETT AND J. D. DELORENZO, Transient scattering by three-dimensional surfaces with wires, *Proc. IEEE International Antenna and Propagation Symp.*, Los Angeles, California, September 22–24, 1971.